Time dependence of ethylene decomposition and byproducts formation in a continuous flow dielectric-packed plasma reactor

ARTICLE *in* CHEMOSPHERE · FEBRUARY 2013

Impact Factor: 3.34 · DOI: 10.1016/j.chemosphere.2013.01.060 · Source: PubMed

5 AUTHORS, INCLUDING:

Mani Sanjeeva Gandhi
Jeju National University
20 PUBLICATIONS **40** CITATIONS
SEE PROFILE

Young Sun Mok
Jeju National University
130 PUBLICATIONS **1,500** CITATIONS
SEE PROFILE

Chemosphere 91 (2013) 685–691

Contents lists available at SciVerse ScienceDirect

Chemosphere

journal homepage: www.elsevier.com/locate/chemosphere

Time dependence of ethylene decomposition and byproducts formation in a continuous flow dielectric-packed plasma reactor

M. Sanjeeva Gandhi [a], Antony Ananth [a], Young Sun Mok [a,*], Jun-Ik Song [b], Kyu-Hyun Park [b]

[a] Department of Chemical and Biological Engineering, Jeju National University, Jeju 690-756, Republic of Korea
[b] National Institute of Animal Science, Rural Development Administration, Suwon 441-706, Republic of Korea

HIGHLIGHTS

- Effectiveness of packing materials was in order of α-Al_2O_3 > SiO_2 > ZrO_2 > glass wool.
- The decomposition efficiency and the BET surface area were deteriorated over time.
- FTIR spectra evidenced the accumulation of polymer-like deposits in the reactor.
- Plasma-mediated regeneration restored the used packing materials to the former states.

ARTICLE INFO

Article history:
Received 25 August 2012
Received in revised form 10 January 2013
Accepted 11 January 2013
Available online 14 February 2013

Keywords:
Plasma
Dielectric-packed bed
Ethylene
Decomposition
Byproducts
Regeneration

ABSTRACT

This work investigated the decomposition of ethylene in a continuous flow dielectric-packed bed plasma reactor filled with various packing materials at atmospheric pressure and room temperature. When compared to the case without any packing material, the reactor filled with packing materials remarkably facilitated the plasma-induced decomposition of ethylene in the order of α-alumina > silica > zirconia > glass wool (GW). Under identical condition, the increase in the decomposition efficiency (DE) with increasing the specific energy input was more rapid in the plasma reactor filled with the packing materials than in the blank plasma reactor. In the early stage, almost complete decomposition of ethylene was observed with the α-alumina, but after a certain period of time, the DE decreased with time. Unlike the α-alumina, the other packing materials examined did not show any significant deterioration in the decomposition over time during 10-h operation. After the regeneration of the used packing materials by using the plasma in the presence of oxygen, the original decomposition performance was nearly recovered. The decrease in the BET surface area due to the formation of polymer deposits was observed in the used α-alumina and silica; however the surface area was almost regained by the regeneration. While no other byproducts except carbon oxides and N_2O were detected with the α-alumina and silica, methane, acetylene, formaldehyde and N_2O were identified in the effluent gas with the zirconia and GW packing materials.

1. Introduction

Ethylene is one of the most prevalent and widely used volatile organic compounds (VOCs) in chemical industries. Secure disposal or reformation of such compounds from the industrial exhausts gains momentum in recent times due to its adverse impacts on the environment and related ecosystems. Lately, non-thermal plasma process combined with catalysis or adsorption is regarded as an energy-efficient technique for the oxidation of VOCs to carbon oxides even at room temperature. The catalyst activation mechanisms under plasma discharge condition include the generation of UV light, ozone formation, local heating, changes in the catalyst working function and adsorption of pollutant and plasma-induced reactive species (Kim et al., 2008). Considerable number of studies described the plasma-catalytic processes for a wide range of application fields which include treatment of solid wastes, soil pollutants, fluorinated compounds, VOCs and water contaminants (Kusic et al., 2005; Vandenbroucke et al., 2011; Wang et al., 2011; Artemov et al., 2012; Gandhi and Mok, 2012).

It has been well documented that the combination of non-thermal plasma with catalysis or adsorption is very effective for promoting oxidative decomposition of VOCs (Song et al., 2002; Van Durme et al., 2008). However, when the porous catalysts or adsorbents are used for long time without regeneration, they generally exhibit deterioration in the performance due to the accumulation of solid deposits which eventually block the micro-pores and the active sites on the surface (Miranda et al., 2007). Besides, deactiva-

* Corresponding author. Tel.: +82 64 754 3680; fax: +82 64 755 3670.
E-mail address: smokie@jejunu.ac.kr (Y.S. Mok).

0045-6535/$ - see front matter © 2013 Elsevier Ltd. All rights reserved.
http://dx.doi.org/10.1016/j.chemosphere.2013.01.060

tion due to catalyst poisoning by reaction product CO_2 is also an important issue that should be taken into account for practical applications (Roland et al., 2005). The above prospective risks prompt the researchers to find a novel technique for regenerating catalysts.

In general, the decomposition rate in a plasma reactor depends on the concentration of target pollutant, discharge power, applied voltage, operating frequency, oxygen content, gas flow rate, etc. In case of the plasma reactor filled with adsorbents or catalysts, the characteristics of the packing material can also significantly affect the behavior of pollutant decomposition and byproducts formation. In the present work, the decomposition of ethylene in a dielectric-packed bed plasma reactor was performed with four different packing materials such as α-alumina, silica, zirconia and glass wool (GW). It is important to note that studies on the regeneration of used packing materials by using the plasma are scarce in the literature. For this reason, an attempt has been made to regenerate the used α-alumina and silica by using the same plasma reactor under oxidative condition. The formation of byproducts, the performance of each packing material, influence of discharge power and changes in the physicochemical properties of the packing materials before and after the decomposition reactions were systematically investigated.

2. Materials and methods

The experiments for the decomposition of ethylene were carried out with a self-designed dielectric-packed bed plasma reactor that is made up of a quartz tube (inner and outer diameter of 21 and 25 mm, respectively) and an 8-mm-thick stainless steel rod electrode. The stainless steel rod serving as a high voltage electrode was coaxially inserted in the quartz tube. The plasma reactor prepared as above was packed with 15 g of different packing materials such as α-alumina, silica, zirconia and GW. Alumina and silica are commonly used catalysts because they have large specific surface areas and porosity. On the other hand, non-porous zirconia and GW have negligible specific surface area. The schematic diagram of the plasma reactor system is shown in Supplementary Material (SM), Fig. SM-1. The whole plasma reactor was enclosed in an acrylic tube filled with circulating water for maintaining room temperature as well as the ground connection to be made. Throughout this work, the decomposition was conducted under room temperature. An alternating current (AC) high voltage of 10–16 kV at a frequency of 400 Hz was applied to the stainless steel rod electrode. The synthetic exhaust gas was prepared with ethylene, nitrogen and oxygen. With maintaining the total flow rate at 1.0 L min^{-1} by using mass flow controllers (MKS Instruments, USA), the oxygen content and the ethylene concentration were controlled to 5 vol.% and 1898 ppmv, respectively. For information, 1.0 ppmv corresponds to 40.9 nM at 298 K. The concentrations of ethylene and derived byproducts were analyzed by an Fourier transform infrared (FTIR) spectrometer (Bruker IFS 66/S, Germany). The decomposition efficiency (DE) of ethylene, CO_x ($CO + CO_2$) selectivity and carbon balance (CB) were calculated by the following equations:

$$\mathrm{DE}\ (\%) = \frac{[C_2H_4]_i - [C_2H_4]_o}{[C_2H_4]_i} \times 100 \quad (1)$$

$$CO_x\ \text{selectivity} = \frac{[CO_2]_o + [CO]_o}{[CO_2]_o + [CO]_o + [HCHO]_o + [CH_4]_o + 2[C_2H_2]_o} \quad (2)$$

$$\mathrm{CB}\ (\%) = \frac{[CO_2]_o + [CO]_o + [HCHO]_o + [CH_4]_o + 2[C_2H_2]_o}{2([C_2H_4]_i - [C_2H_4]_o)} \quad (3)$$

where the brackets stand for concentration in ppmv, and subscripts *i* and *o* designate the reactor inlet and outlet, respectively.

The effect of the type of packing material on the decomposition of ethylene was examined in two phases; the first phase of the experiments was conducted by changing the input power while the long-term stabilities of the packing materials were investigated in the second phase by operating the plasma reactor continuously for 10 h. For the regeneration, the used α-alumina and silica were treated in the plasma reactor in the presence of only oxygen for 2 h at an input power of 100 W. The fresh and regenerated packing materials were characterized by the FTIR spectrometer and a BET surface area analyzer (Quantachrome, AUTOSORB-1-MP). Since ZrO_2 and GW display negligible surface area and less probability to accumulate solid deposits, they need not be considered for the regeneration. The BET surface areas of zirconia and glass wool were measured to be 2 and 1 $m^2\ g^{-1}$, indicating that they have negligible adsorption capabilities.

The input power was monitored by using a digital power meter (Model WT200, Yokogawa, Japan). The power dissipated in the plasma reactor (discharge power) was determined from the area of the Lissajous curve generated in the oscilloscope (Tektronix MSO/DPO3000) (Mok and Kim, 2011). The specific energy input (SEI) was defined as follows:

$$\mathrm{SEI(J/L)} = \frac{\text{Discharge power (W)}}{\text{Gas flow rate (L/s)}} \quad (4)$$

The DE of ethylene with different packing materials was compared as a function of SEI.

3. Results and discussions

3.1. Dependence of discharge power on the type of packing material

The discharge power of the blank plasma reactor was relatively low, compared to the cases with the packing materials, as represented in Fig. SM-2. This might be because the presence of the packing material in the plasma reactor in effect increases the average electric field intensity, thereby reducing the discharge ignition voltage (Tu et al., 2011). Among the packing materials investigated, the α-alumina and silica with porous structure exhibited significantly higher discharge power than the zirconia and GW. This result is obviously because numerous micro-discharges occurred not only in the gas phase but also in the micro-pores. Hensel et al. (2007) reported that micro-discharge formation inside porous ceramics represents a novel way to generate large-volume, stable atmospheric pressure plasmas. Cho et al. (2008) have shown that the discharge utilizing nanoporous dielectric barrier is more uniform, displays lower discharge ignition voltage and more energy efficient in ozone generation than the discharge through smooth-surface dielectric barriers. According to Takaki et al. (2004), the discharge power can also be affected by the dielectric constant of packing material. They have shown that the discharge power increases with increasing dielectric constant of packing material from 660 to 10,000. The dielectric constants of the packing materials investigated in this work are 9.0, 3.9, 25 and 3.4 for α-alumina, silica, zirconia and GW, respectively (Robertson, 2004; Dudeja, 2010). In this dielectric constant range, it is thought that the discharge power is mainly determined by the porosity of the packing material rather than by the dielectric constant.

3.2. Ethylene decomposition and the by-product distribution

The effect of the type of packing material on the decomposition of ethylene as a function of SEI is depicted in Fig. 1a. When the decomposition was performed with the blank reactor, it was

observed that the DE rapidly increased with increasing the SEI up to 1830 J L^{-1} and then slowed down at higher SEI. While the blank reactor decomposed about 78% of the ethylene throughput at an SEI 1830 J L^{-1}, the reactor packed with the α-alumina or silica achieved almost complete decomposition at much lower SEI of 1020 and 1060 J L^{-1}, respectively. For information, the GW and zirconia required approximately 1900 J L^{-1} for the complete decomposition. For the sake of understanding, the decomposition tendency of the packing materials can be distinguished into group I (α-alumina and silica) and group II (zirconia and GW) on the basis of the behavioral similarity, i.e., similar characteristics such as the input power vs. discharge power (Fig. SM-2) and the SEI vs. DE (Fig. 1a). The decomposition behavior is believed to be closely related to the surface areas of the packing materials. The group I packing materials such as α-alumina and silica have large specific surface areas capable of accommodating ethylene by adsorption, and the numerous micro-discharges occurring in the micro-pores can readily decompose the adsorbed ethylene. A merit of the presence of adsorbent or catalyst in the plasma reactor is to speed up chemical reactions which are relatively slow or impossible in the gas phase, because molecules adsorbed on the surface are much more likely to be attacked by the reactive species generated by the plasma than those in the gas phase. That is why industrial catalysts have high surface areas. There is also another reason for adsorbent or catalyst to speed up chemical reactions, which can be interpreted by the bond dissociation energy of a molecule. Chemical bond of a molecule is weakened upon adsorption on the surface (Bradford and Vannice, 1996), which means that the bond more easily dissociates when the molecule collides with the reactive species generated by the plasma. Moreover, when the molecules are enriched on the surface, the reactive species can be more efficiently utilized than when the molecules wander about in the gas phase. In Fig. 1a, such higher DE of the group I packing materials can be explained in this way.

The formation of byproducts in the plasma reactor was also affected by the packing materials used. The concentration of the byproducts at an identical input power of 45 W is depicted in the Fig. 1b. As can be seen in this figure, considerable amounts of methane and acetylene were identified as byproducts when the GW and zirconia were filled in the plasma reactor. In addition, formaldehyde was also detected in the effluent gas as a minor byproduct (Fig. SM-3). These observations are in good agreement with the previous study by Liao et al. (2005) who observed the formation of acetylene, methane and formaldehyde by the non-thermal plasma degradation of ethylene oxide. On the other hand, the α-alumina and silica-packed reactors did not produce all the aforementioned byproducts, implying that the group I packing materials help the degradation process move towards total oxidation. Complete oxidation of ethylene in the presence of O_2 can be described as follows:

$$C_2H_4 + 3O_2 \rightarrow 2CO_2 + 2H_2O \quad (5)$$

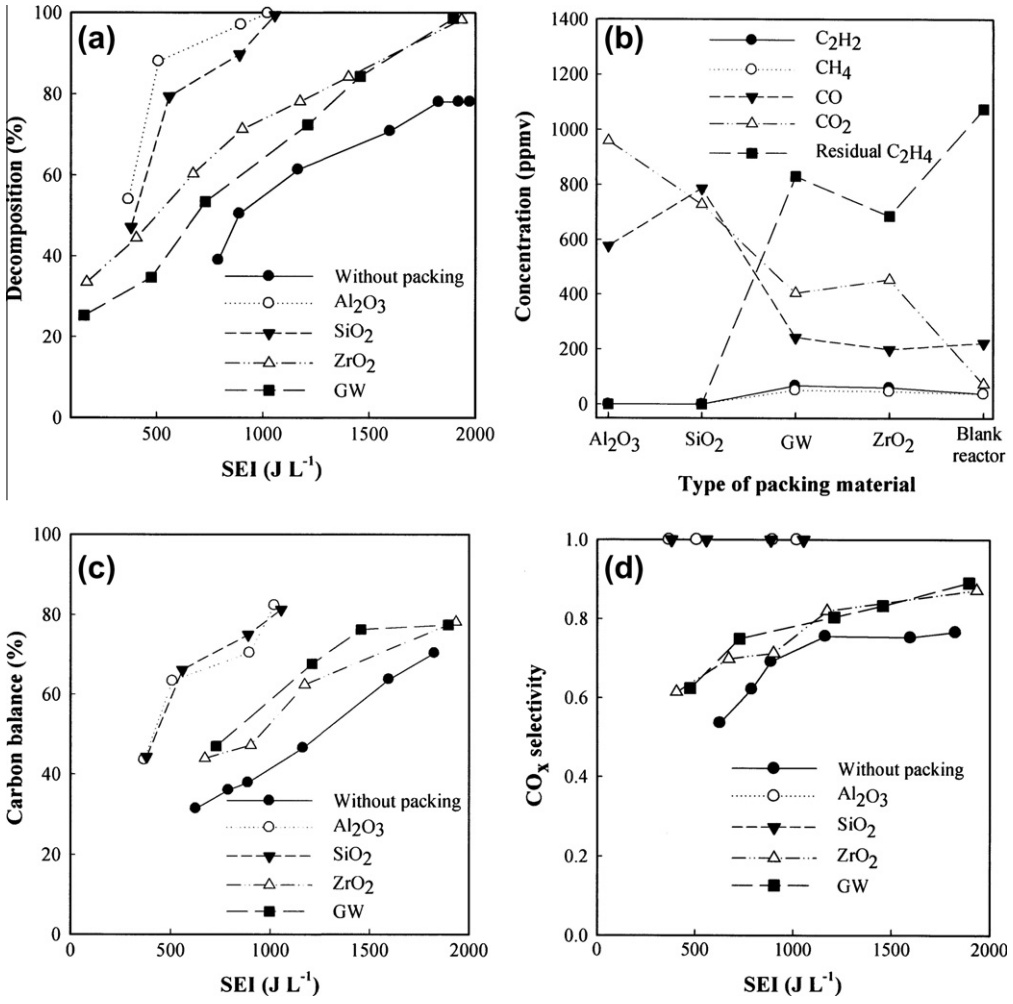

Fig. 1. Effect of the type of packing material on the decomposition of ethylene (a), the formation of byproducts (b), carbon balance (c) and CO_x selectivity (d).

Even though the most desirable mode of ethylene decomposition is the oxidation to CO_2, unwanted byproducts are also formed. The decomposition of ethylene in the plasma reactor goes through several steps, which is summarized in Table 1 (Mallard et al., 1998). During the electrical discharge, N_2 and O_2 molecules produce a variety of reactive species such as $N_2\left(A^3\sum_u^+\right)$, O, N and O_3 in collisions with electrons. These reactive species initiate the decomposition of ethylene to form fragments such as C_2H_3, C_2H_2, CH_2O and CH_3 (R1–R5 in Table 1). Note that C_2H_3 and CH_3 are vulnerable to oxidation because they are chemically unstable. By reactions R6–R15, C_2H_3 and CH_3 are converted into C_2H_2 and CH_2O. The formation of CH_4 can be explained by R22–R24, As easily understood in Table 1, C_2H_2 and CH_2O are key intermediate products leading to CO and CO_2. In oxidation atmosphere, these intermediate species can be further oxidized to form CO and CO_2 via various reactions.

Fig. 1c and d shows the carbon balance and the CO_x selectivity as a function of SEI. As can be seen in the Fig. 1c, the increase in the SEI leads to higher CB. Among the tested packing systems, the group I materials showed better CB than the group II materials. The CB below 100% indicates that some unidentified byproducts deposited on the surface of the packing material. Poor carbon balance of 63–90% for plasma decomposition of organic compounds was earlier documented by Kim et al. (2004), who reported a large quantity of nanometer-sized aerosols was formed in the reactor. In addition to the DE and CB, the group I materials exhibited much higher CO_x selectivity than the group II packing materials (Fig. 1d), suggesting that the α-alumina and silica catalyzed the oxidation of intermediate products. The poor CO_x selectivity of the group II packing materials is attributed to the formation of acetylene, formaldehyde and methane, as understood from Fig. 1b.

The long-term stabilities of the packing materials were investigated for 10 h. The SEI was 1020 J L^{-1} for α-alumina and silica, and 2340 J L^{-1} for GW and zirconia. All the investigated packing materials except the α-alumina maintained steady decomposition rates during the 10-h operation. In case of the α-alumina-packed reactor, however, the DE was getting decreased after a certain period of time, revealing 11% decrease in the DE in 10 h, which is obviously because the accumulation of solid deposits generated from ethylene deactivated the α-alumina. The silica has much larger BET surface area than the α-alumina (Table 2). In other words, the silica can withstand the deactivation for longer time, which can explain the steady decomposition rate during the 10-h operation. Although the zirconia and GW did not show any significant deterioration in the decomposition over time during the operation, it should be noted that they required more energy than the α-alumina to achieve a given DE.

Fig. 2a–d shows the concentrations of the byproducts obtained with the α-alumina, silica, GW and zirconia, respectively. When the GW and zirconia were used, the concentrations of the byproducts did not fluctuate much throughout the 10-h operations. Unlike the GW and zirconia, the α-alumina and silica packing materials resulted in significant variations in the concentrations of the byproducts. These variations may be explained by the blockages of the micro-pores and the active sites of the α-alumina and silica due to the formation and accumulation of solid deposits. The results also suggest that the GW and zirconia did not act as catalysts. Since the zirconia and GW with BET surface areas less than 2 m^2 g^{-1} have negligible adsorption capabilities, i.e., negligible catalytic activities, the decomposition of ethylene primarily takes place in the gas phase and the accumulation of solid deposits on the surface of packing materials hardly affect the decomposition and the formation of byproducts. Meanwhile, with the α-alumina and silica packing materials, longer treatment time led to the formation of more CO instead of CO_2, which may be attributed to the deactivation of the α-alumina and silica. As well as the solid deposits, oxygenated byproducts such as acetylene and formaldehyde resulting from incomplete oxidation of ethylene may also be responsible for the deactivation, which is in line with the findings of Roland et al. (2005).

Table 1
Chemical reactions related to the ethylene decomposition (Mallard et al., 1998).

Reaction	Rate constant at 298 K (cm^3 mol^{-1} s^{-1})
Initiation of ethylene decomposition	
R1	C_2H_4 + energetic species $\left(e^-, N_2\left(A^3\sum_u^+\right)\right)$ $\rightarrow C_2H_3 + H$
R2	C_2H_4 + energetic species $\left(e^-, N_2\left(A^3\sum_u^+\right)\right)$ $\rightarrow C_2H_2 + H_2$
R3	$C_2H_4 + O_3 \rightarrow CH_2O + CH_2O + O$	1.06×10^6
R4	$C_2H_4 + N \rightarrow HCN + CH_3$	2.53×10^{10}
R5	$C_2H_4 + O \rightarrow C_2H_3 + OH$	1.49×10^9
Formation of byproducts	
R6	$C_2H_3 + O_2 \rightarrow C_2H_2 + HO_2$	2.46×10^{10}
R7	$C_2H_3 + O_2 \rightarrow CH_2CHO + O$	5.71×10^{10}
R8	$CH_2CHO + O_2 \rightarrow CH_2O + CO + OH$	1.81×10^{10}
R9	C_2H_2 + energetic species $\left(e^-, N_2\left(A^3\sum_u^+\right)\right) \rightarrow C_2H + H$	
R10	$C_2H + O_2 \rightarrow HCO + CO$	2.41×10^{12}
R11	$CH_3 + O_2 \rightarrow CH_3O_2$	1.63×10^{17}
R12	$CH_3O_2 + O \rightarrow CH_3O + O_2$	2.59×10^{13}
R13	$CH_3 + O \rightarrow CH_2O + H$	5.66×10^{13}
R14	$CH_3O + O_2 \rightarrow CH_2O + HO_2$	1.15×10^9
R15	$CH_3O + O \rightarrow CH_2O + OH$	6.03×10^{12}
R16	$CH_2O + O \rightarrow HCO + OH$	1.01×10^{11}
R17	$HCO + O_2 \rightarrow CO + HO_2$	3.37×10^{12}
R18	$HCO + O \rightarrow CO_2 + H$	3.01×10^{13}
R19	$HCO + O \rightarrow CO + OH$	3.01×10^{13}
R20	$CO + O(^1D) \rightarrow CO_2$	4.82×10^{13}
R21	$CO + O \rightarrow CO_2$	3.88×10^{12}
R22	$CH_3 + H \rightarrow CH_4$	1.22×10^{14}
R23	$CH_3 + C_2H_3 \rightarrow CH_4 + C_2H_2$	2.05×10^{13}
R24	$CH_3 + HCO \rightarrow CH_4 + CO$	2.65×10^{13}

3.3. Characterization of the regenerated packing materials

Reusability of the packing materials may be an important issue for practical applications to industrial effluent gases. For the regeneration, the α-alumina and silica used in the above decomposition experiments (for 10 h at an SEI of 1020 J L^{-1}) were post-treated as per the procedures described above. The regeneration of the packing materials includes the elimination of the solid deposits and the oxygenated byproducts that block the micro-pores and the active sites. As shown in Fig. 3, the regenerated α-alumina and silica achieved as good DE as the fresh ones. The regenerated packing materials were found to show only slight decrements in the DE, implying that they were not fully regenerated. The characteristics

Table 2
BET surface areas of the packing materials.

Sample	BET surface area (m^2 g^{-1})	Average pore radius (Å)	Total pore volume (cm^3 g^{-1})
α-Al_2O_3 – fresh	348	28.6	0.450
α-Al_2O_3 – after 10 h	303	25.9	0.417
α-Al_2O_3 – after regeneration	320	26.1	0.434
SiO_2 – fresh	649	12.0	0.391
SiO_2 – after 10 h	597	11.6	0.347
SiO_2 – after regeneration	643	11.9	0.383

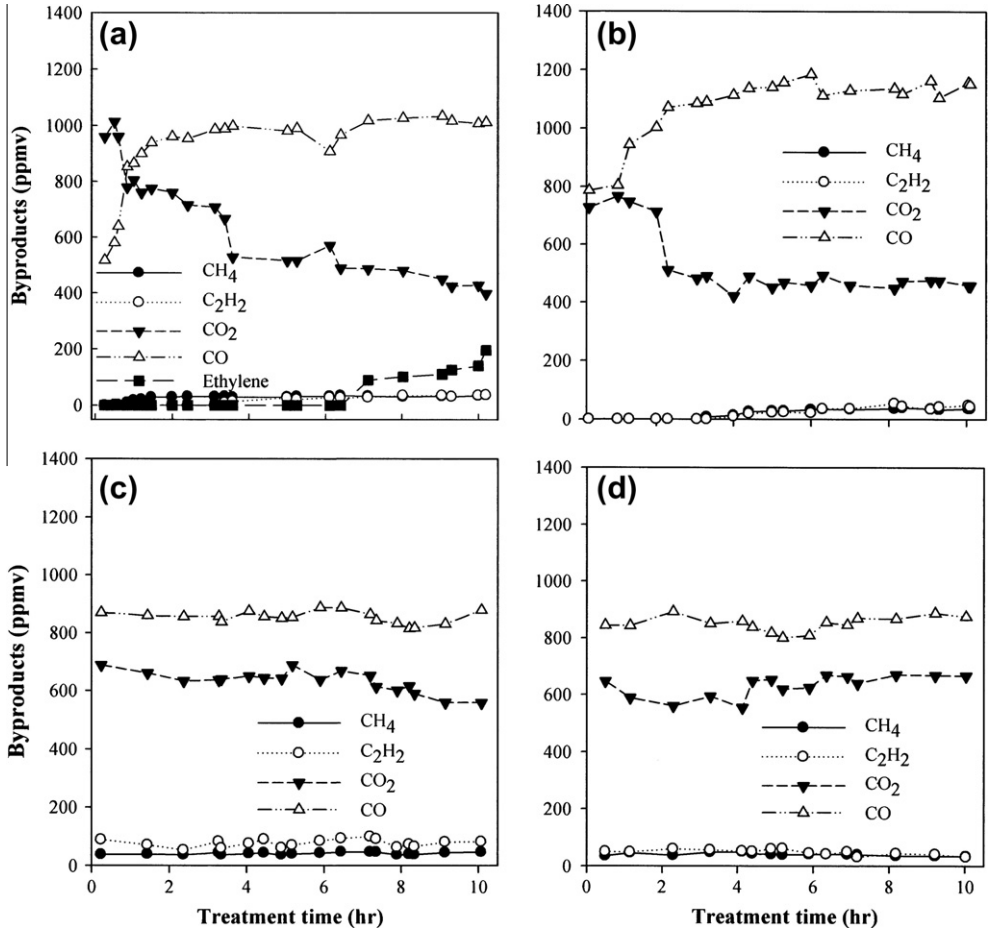

Fig. 2. Temporal variations in the concentrations of byproducts under (a) α-alumina, (b) silica, (c) glass wool and (d) zirconia SEI: 1020 J L^{-1} for α-alumina and silica; 2340 J L^{-1} for GW and zirconia.

of the fresh, used and regenerated packing materials are discussed below.

The BET surface area, average pore size and total pore volume of the α-alumina and silica before and after the plasma treatment are summarized in Table 2. The BET surface areas of the fresh α-alumina and silica were measured to be 348 and 649 m^2 g^{-1}, respectively. After the 10-h operation, the surface areas of the α-alumina and silica decreased to 303 and 597 m^2 g^{-1}, respectively. This is about 13% and 8% decrement as compared to the fresh ones. Besides, the average pore radius and the total pore volume also decreased after the 10-h operation. The decrease in the surface area, pore size and volume after the long-term operation is obviously due to the accumulation of solid deposits. The solid deposits may be a mixture of various polymer-like compounds that can be removed during the oxidative regeneration step. As can be seen in Table 2, the surface area, pore size and volume were almost regained upon the regeneration but not completely. For complete regeneration, prolonged regeneration time is needed.

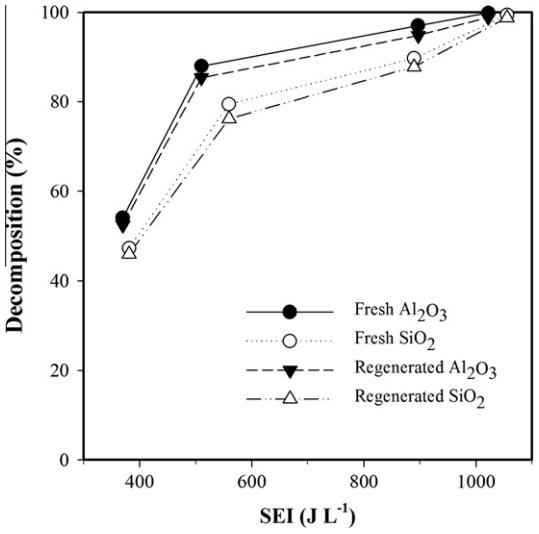

Fig. 3. Comparison of the decomposition efficiencies between the fresh and the regenerated packing materials.

After the 10-h operation, the α-alumina and silica exhibited visible changes in their colors to light yellowish brown. The FTIR studies further confirmed the existence of polymer-like compounds on the surface of the used packing materials. Fig. 4a shows the FTIR spectra of the fresh, used and regenerated α-alumina. The smooth and broad band around 400–1017 cm^{-1} represents the stretching vibration of Al–O–Al. The broadening of this region accounts for the distribution of vacancies between the octahedral and tetrahedral sites of Al–O–Al (Costa et al., 1999). The broad band centered at 3500 cm^{-1} results from the O–H stretching vibration. After the 10-h operation, an important characteristic peak of C–H at 1383 cm^{-1} was noticed in the spectrum, which indicates the Al–O–Al linkages with C–H. It is inferred from the spectrum that the outer layer of the used α-alumina has been covered by polymer-

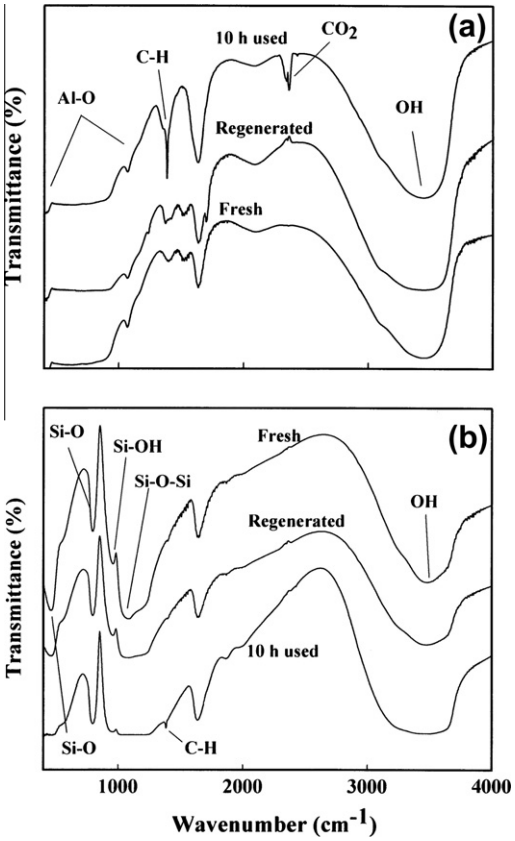

Fig. 4. FTIR spectra of the fresh, used and regenerated α-alumina (a) and silica (b).

like solid deposits. In addition, the intensities of resonance peaks such as O–H and CO_2 (at 1625 and 2345 cm^{-1}, respectively) slightly increased after the 10-h operation. The above noticed changes suggest that the α-alumina absorbs some amount of OH and CO_2 during the ethylene decomposition process. The characteristic FTIR spectra of the fresh, used and regenerated silica are depicted in Fig. 4b. The bands around 450 cm^{-1} can be attributed to Si–O out of plane deformation and a band located at 800 cm^{-1} is attributed to the vibration of Si–O bending. The peak at 950 cm^{-1} is due to the O–H stretching vibration of Si–OH bond (Hamelmann et al., 2005). It should be noted that the characteristic peak for C–H deformation is located at around 1268–1395 cm^{-1}. Upon the regeneration step, the used α-alumina and silica recovered their original spectra.

4. Conclusions

The decomposition of ethylene was carried out using the plasma reactor filled with the α-alumina, silica, zirconia and GW. Among the packing materials, the α-alumina exhibited the best decomposition performance; however the DE gradually decreased after a certain period of time because it was deactivated by the accumulation of polymer-like solid deposits. After the longtime operation, the packing materials underwent visible changes in their colors to light yellowish brown and considerable reductions in the specific surface areas. When the used packing materials were regenerated by the plasma under oxidative condition, the DE as well as the BET surface area was nearly restored to the former state. Different from the α-alumina showing deterioration in the DE over time, the GW and zirconia without any catalytic activity maintained steady decomposition rates throughout the 10-h operation, regardless of the accumulation of the yellowish solid deposits. The plasma reactor filled with the GW or zirconia produced substantial amounts of byproducts such as methane, acetylene and formaldehyde, whereas the α-alumina and silica enhanced the conversion of ethylene to CO and CO_2. Moreover, good carbon balance and selectivity to carbon oxides were obtained with the α-alumina and silica packing materials.

Acknowledgement

This work was carried out with the support of "Cooperative Research Program for Agriculture Science & Technology Development (Project No. PJ008508032012)", Rural Development Administration, Republic of Korea.

Appendix A. Supplementary material

Supplementary data associated with this article can be found, in the online version, at http://dx.doi.org/10.1016/j.chemosphere.2013.01.060.

References

Artemov, A.V., Bulba, V.A., Voshchinin, S.A., Krutyakov, Y.A., Kudrinskii, A.A., Ostryi, I.I., Pereslavtsev, A.V., 2012. Catalytic transformations of gaseous products of plasma treatment of solid wastes and hydrocarbon raw materials. Russ. J. Gen. Chem. 82, 791–800.

Bradford, M.C.J., Vannice, M.A., 1996. Estimation of CO heats of adsorption on metal surfaces from vibrational spectra. Ind. Eng. Chem. Res. 35, 3171–3178.

Cho, J.H., Koo, I.G., Choi, M.Y., Lee, W.M., 2008. Ozone production by nanoporous dielectric barrier glow discharge in atmospheric pressure air. Appl. Phys. Lett. 92, 101504.

Costa, T.M.H., Gallas, M.R., Benvenutti, E.V., Da Jornada, J.A.H., 1999. Study of nanocrystalline γ-Al_2O_3 produced by high-pressure compaction. J. Phys. Chem. B 103, 4278–4284.

Dudeja, R.R., 2010. Electrostatics and Electricity, In: The Pearson Guide to Objective Physics for the AIEEE, third ed. Dorling Kindersley Pvt. Ltd., India.

Gandhi, M.S., Mok, Y.S., 2012. Decomposition of trifluoromethane in a dielectric barrier discharge non-thermal plasma reactor. J. Environ. Sci. 24, 1234–1239.

Hamelmann, F., Heinzmann, U., Szekeres, A., Kirov, N., Nikolova, N., 2005. Deposition of silicon oxide thin films in TEOS with addition of oxygen to the plasma ambient: IR spectra analysis. J. Optoelectron. Adv. Mater. 7, 389–392.

Hensel, K., Martisovits, V., Machala, Z., Janda, M., Lestinsky, M., Tardiveau, P., Mizuno, A., 2007. Electrical and optical properties of AC microdischarges in porous ceramics. Plasma Process. Polym. 4, 682–693.

Kim, H.H., Ogata, A., Futamura, S., 2004. Decomposition of gas-phase benzene using hybrid systems of a non-thermal plasma and catalysts. J. Kor. Phys. Soc. 44, 1163–1167.

Kim, H.H., Ogata, A., Futamura, S., 2008. Oxygen partial pressure-dependent behavior of various catalysts for the total oxidation of VOCs using cycled system of adsorption and oxygen plasma. Appl. Catal. B-Environ. 79, 356–367.

Kusic, H., Koprivanac, N., Locke, B.R., 2005. Decomposition of phenol by hybrid gas/liquid electrical discharge reactors with zeolite catalysts. J. Hazard. Mater. 125, 190–200.

Liao, W.T., Wei, T.C., Hsieh, L.T., Tsai, C.H., Shih, M., 2005. Reaction mechanism of ethylene oxide at various oxygen/ethylene oxide ratios in an RF cold plasma environment. Aerosol Air. Qual. Res. 5, 185–203.

Mallard, W.G., Westley, F., Herron, J.T., Hampson, R., 1998. National Institute of Standards and Technology (NIST) Chemical Kinetics Database: Version 2Q98.

Miranda, B., Diaz, E., Ordonez, S., Vega, A., Diez, F.V., 2007. Oxidation of trichloroethene over metal oxide catalysts: Kinetic studies and correlation with adsorption properties. Chemosphere 66, 1706–1715.

Mok, Y.S., Kim, D.H., 2011. Treatment of toluene by using adsorption and nonthermal plasma oxidation process. Curr. Appl. Phys. 11, 58–62.

Robertson, J., 2004. High dielectric constant oxides. Eur. Phys. J. Appl. Phys. 28, 265–291.

Roland, U., Holzer, F., Kopinke, F.D., 2005. Combination of non-thermal plasma and heterogeneous catalysis for oxidation of volatile organic compounds Part 2. Ozone decomposition and deactivation of α-Al_2O_3. Appl. Catal. B-Environ. 58, 217–226.

Song, Y.H., Kim, S.J., Choi, K.I., Yamamoto, T., 2002. Effects of adsorption and temperature on a non-thermal plasma process for removing VOCs. J. Electrostat. 55, 189–201.

Takaki, K., Chang, J.S., Kostov, K.G., 2004. Atmospheric pressure of nitrogen plasmas in a ferro-electric packed bed barrier discharge reactor part I: modeling. IEEE Trans. Dielect. Electr. Insul. 11, 481–490.

Tu, X., Verheyde, B., Corthals, S., Paulussen, S., Sels, B.F., 2011. Effect of packing solid material on characteristics of helium dielectric barrier discharge at atmospheric pressure. Phys. Plasmas 18, 080702.

Van Durme, J., Dewulf, J., Leys, C., Van Langenhove, H., 2008. Combining non-thermal plasma with heterogeneous catalysis in waste gas treatment: a review. Appl. Catal. B-Environ. 78, 324–333.
Vandenbroucke, A.M., Morent, R., Geyter, N.D., Leys, C., 2011. Non-thermal plasmas for non-catalytic and catalytic VOC abatement. J. Hazard. Mater. 195, 30–54.
Wang, T., Lu, N., Li, J., Wu, Y., Su, Y., 2011. Enhanced degradation of p-nitrophenol in soil in a pulsed discharge plasma-catalytic system. J. Hazard. Mater. 195, 276–280.